JOURNAL OF SOLID STATE CHEMISTRY 35, 347–356 (1980)

Studies on the Compounds in Ba–Fe–S System. II. Disordered Intergrowth Structure in $Ba_3Fe_{1+x}S_5$ ($\frac{1}{3} \leq x \leq \frac{2}{5}$) Observed by Electron Microscopy

N. NAKAYAMA, K. KOSUGE, AND S. KACHI

Department of Chemistry, Faculty of Science, Kyoto University, Kyoto 606, Japan

Received October 30, 1979; in revised form March 6, 1980

Shattered crystallites of $Ba_3Fe_{1+x}S_5$ ($\frac{1}{3} \leq x \leq \frac{2}{5}$) were examined by electron microscopy. Both β-$Ba_9Fe_4S_{15}$ ($x = 0.333$) and $Ba_{15}Fe_7S_{25}$ ($x = 0.40$), previously reported members of $Ba_{3p}Fe_qS_{5p}$ series, were identified by electron diffraction patterns, and supercell periodicities, 25.5 Å ($\simeq 3a_0$) and 42.0 Å ($\sim 5a_0$), respectively, were resolved as lattice fringes. Some crystals with intermediate compositions showed electron diffraction patterns with diffuse superlattice reflections. Their lattice fringe patterns showed a microscopic disordered intergrowth structure consisting of three periodicities, $3a_0$, $5a_0$, and $4a_0$. The intergrowth structure is a disordered one and can be analyzed based on the one-dimensional disorder model of Fe occupation in the hexagonal rings of the Ba_3S_5 framework. It is also characteristic of the "microsyntactic" intergrowth.

Introduction

Two homologous series of compounds, $Ba_{3p}Fe_qS_{5p}$ (*1, 2*) and $Ba_p(Fe_2S_4)_q$ (*3, 4*) (p, q: integer), have been reported in the ternary Ba–Fe–S system. The compounds in both series have complex long-period superstructures and many compounds with different supercell periodicities exist nearly continuously in a narrow composition range, i.e., $0 \leq x \leq 0.40$ for $Ba_3Fe_{1+x}S_5$ and $0.0625 \leq x \leq 0.143$ for $Ba_{1+x}Fe_2S_4$. In this sense, both series are known as examples of "infinitely adaptive" series, a term recently coined by J. S. Anderson (*5, 6*). To characterize such complex phases, electron microscopy is a powerful tool, but no such work has been reported for these series yet. We report here (Part II) the results of electron diffraction and electron microscopic observations for $Ba_3Fe_{1+x}S_5$. The results for $Ba_{1+x}Fe_2S_4$ will be published elsewhere in the near future (Parts III, IV).

Structure Aspect of $Ba_{3p}Fe_qS_{5p}$ Series

Three members of the $Ba_{3p}Fe_qS_{5p}$ series have been confirmed by single-crystal X-ray studies (*1, 2*), that is, Ba_3FeS_5 ($x = 0$), β-$Ba_9Fe_4S_{15}$ ($x = \frac{1}{3}$), and $Ba_{15}Fe_7S_{25}$ ($x = \frac{2}{5}$). The structures of β-$Ba_9Fe_4S_{15}$ and

0022-4596/80/150347-10$02.00/0

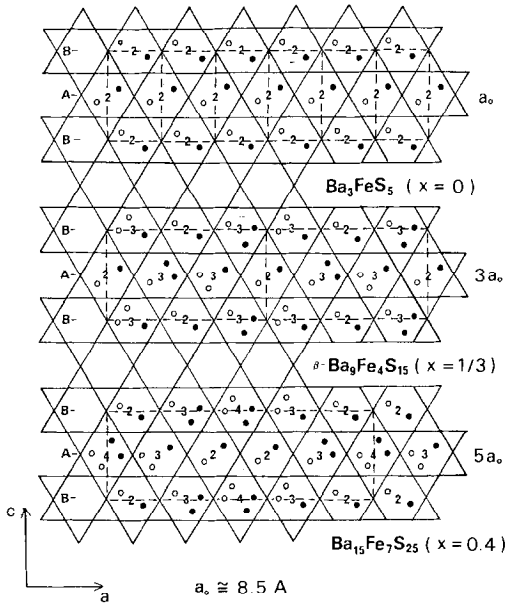

FIG. 1. Schematic representation of the supercell of the $Ba_{3p}Fe_qS_{5p}$ series. The Ba_3S_5 framework (hexagonal rings) is shown by solid lines and the unit cell of superstructure is shown by dashed lines. The Fe atoms in the hexagonal rings are represented by circles and the number of Fe atoms in a ring α is also shown in the figure. For the detail of the structure, see Refs. (*1, 2*).

$Ba_{15}Fe_7S_{25}$ are superstructures based on the structure of Ba_3FeS_5 (high-pressure phase). They are shown schematically in Fig. 1.

The basic structure is described based on the articulation of BaS_6 trigonal prisms in a manner similar to the description of other compounds in the Ba–Fe–S system (*7, 8*). BaS_6 trigonal prisms share their edges and triangular faces, and create hexagonal enclosures (hexagonal rings). Within the rings are additional Ba and S and, thus, tetrahedral interstices are created that can be filled with Fe atoms (Ba_3S_5 framework). There are six available sites for Fe in a ring and a group of three tetrahedra link by face sharing. Judging from the structure analyzed by Steinfink and coworkers (*1, 2*), there exist only three types of Fe occupancy. α, the number of occupied Fe sites can take on the value 2, 3, or 4. In a ring with two Fe, two central tetrahedral interstices are occupied. In Ba_3FeS_5, Fe occupancies are all of this type. In a ring with four Fe, four outside ones are occupied. In a ring with three Fe, one central and two outside opposite ones are occupied. The variation of the Fe occupancy in the successive rings gives rise to the phases, β-$Ba_9Fe_4S_{15}$ and $Ba_{15}Fe_7S_{25}$. The sequence of Fe occupation numbers α along the a axis is 2–3–3 in β-$Ba_9Fe_4S_{25}$ and 2–3–4–3–2 in $Ba_{15}Fe_7S_{25}$. Then the unit cell dimension a is close to $3a_0$ and $5a_0$, respectively, where a_0 is the a dimension of the Ba_3S_5 framework or the c dimension of the Ba_3FeS_5 cell. The unit cell contains two arrays (A, B: see Fig. 1) of hexagonal rings. The "phase" of the sequence of Fe occupation number α differs in these two neighboring arrays of hexagonal rings by half of the unit cell dimension, a. However the orientation of occupied Fe sites is different between the A and B array and the relationship is that of the space group. *Pnma*. Cohen *et al.* (*2*) predicted the existence of many compounds in the composition range $\frac{1}{3} \leq x \leq 1$ based on the above structure principle, and called them an "infinitely adaptive" series. The low-temperature form of $Ba_9Fe_4S_{15}$ (α form) was also reported (*2*) but its strcuture is a more complex one that cannot be described by the above structure principle.

Experimental

The samples were prepared by heating powder mixtures of BaS, Fe, and S, which were enclosed in graphite crucibles to avoid reaction with silica, inside evacuated silica tubes. Mixtures with starting composition, $x = 0.33, 0.40, 0.43$, and 0.50 in $Ba_3Fe_{1+x}S_5$, were heated at 350°C for 1 day and then at 900°C for 2 weeks. A slight excess of sulfur was added following Cohen *et al.* (*2*). Obtained products were crushed, pressed into

pellet form, and again annealed at 900°C for 2 weeks. Another mixture with $x = 0.40$ was heated at 1000°C in order to investigate the effect of annealing temperature. Obtained products were identified by X-ray powder diffraction. No strong reflections indicating the existence of a second phase were observed. X-Ray powder diffraction patterns showed no appreciable difference due to the difference of starting compositions. They showed the strong reflections related to the basic Ba_3FeS_5 cell and supercell reflections were too weak to analyze.

For electron microscopic observation, samples were finely crushed between two glass plates and dispersed into methyl alcohol. Then, they were collected on a Collodion microgrid with small holes, coated by carbon and mounted on a copper mesh. Electron diffraction patterns and images were observed using a JEM-7A electron microscope equipped with a goniometer stage operating under 120-kV electron radiation. Very thin crystals were selected and tilted so as to give the diffraction containing a^* in reciprocal space.

Results

1. Two Members of the $Ba_{3p}Fe_qS_{5p}$ Series: β-$Ba_9Fe_4S_{15}$ and $Ba_{15}Fe_7S_{25}$

Many of the obtained electron diffraction patterns were those of two previously reported members of the $Ba_{3p}Fe_qS_{5p}$ series, β-$Ba_9Fe_4S_{15}$ and $Ba_{15}Fe_7S_{25}$. Most of the sample with starting composition $x = 0.43$ and 0.50 gave electron diffraction patterns of $Ba_{15}Fe_7S_{25}$. Those of β-$Ba_9Fe_4S_{15}$ were observed most often in the sample with $x = 0.40$ annealed at 1000°C. Typical examples of the (010)* reciprocal plane are shown in Fig. 2a. Some basic spots related to the Ba_3FeS_5 basic cell are marked by arrows. Along the a^* axis, diffraction spots show arrays with the spacing corresponding to the lengths 25.5 and 42.0 Å in real space, which are the a dimensions of β-$Ba_9Fe_4S_{15}$ and $Ba_{15}Fe_7S_{25}$, respectively. The superlattice spots divide the distance between the two basic spots along the a^* axis into three and five equal parts, respectively, which indicates the supercell periodicity to be $3a_0$ and $5a_0$, respectively. The violation of the extinction condition, $hk0$; $h = 2n + 1$ (*1, 2*), in the $h00$ row is due to the double diffraction effect. Also, the violation of the extinction condition, $0kl$; $k + 1 = 2n + 1$ (*1, 2*), in the 001 row is due to the same effect. Bright-field images of the crystal showing these diffraction patterns are shown in Fig. 2b. The incident beam is parallel to the b axis and the diffraction spots used for imaging are indicated in the figure. The lattice fringes were observed with the spacing 25.5 and 42.0 Å, respectively.

2. Miscroscopically Disordered Intergrowth Structure

In some diffraction patterns ($\simeq 20\%$ of obtained diffraction patterns) superlattice spots showed diffuse streaks, while the main spots corresponding to the Ba_3S_5 framework did not show such behavior, as shown in the inset of Fig. 3. These diffraction patterns were observed most often in the sample with starting compositions $x = 0.33$ and 0.40 annealed at 900°C, in which those of β-$Ba_9Fe_4S_{15}$ and $Ba_{15}Fe_7S_{25}$ were also observed with nearly equal probabilities. This fact shows that the Fe composition x of the crystal showing diffuse streaks is intermediate between those of β-$Ba_9Fe_4S_{15}$ ($x = 0.333$) and $Ba_{15}Fe_7S_{25}$ ($x = 0.40$).

The diffuse streaks usually showed their intensity maxima near the main spots. It seems that these diffraction patterns indicate the coexistence of different structure variants in a crystal. Bright-field images of the crystals giving such diffraction patterns showed disordered lattice fringes or many

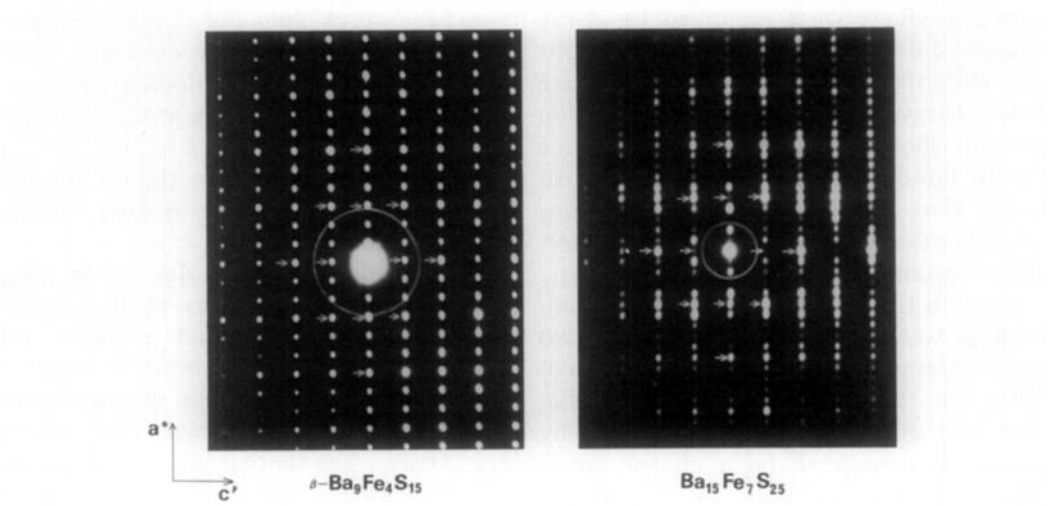

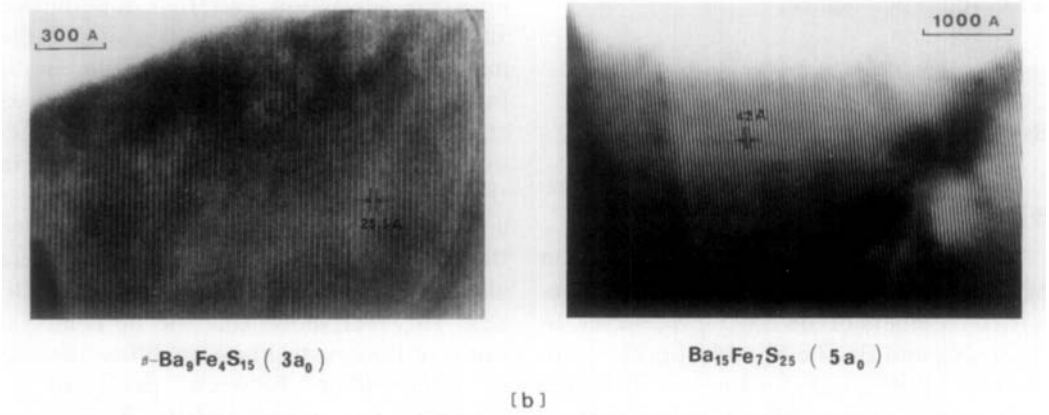

FIG. 2. Electron diffraction patterns and lattice fringe images of β-$Ba_9Fe_4S_{15}$ and $Ba_{15}Fe_7S_{25}$. (a) (010)* electron diffraction patterns. Some basic spots corresponding to the Ba_3S_5 framework or Ba_3FeS_5 cell are marked by arrows. (b) Bright-field images of thin fragment ((010) incidence). Diffraction spots used for imaging are shown in (a).

defects. Their interfringe spacings were the mixture of three periods, 42 Å ($\simeq 5a_0$), 25.5 Å ($\simeq 3a_0$), and 33 Å ($\simeq 4a_0$). Often, bundles of lattice fringes with a different shade were observed and the bundle with the different shade had different interfringe spacings. Figure 3a shows a two-dimensional lattice fringe image of the crystal, indicating one-dimensional disordered lattice fringes parallel to the a axis. Interfringe spacings perpendicular to the a axis, however, were constant (12.5 Å = c) and no defects were observed.

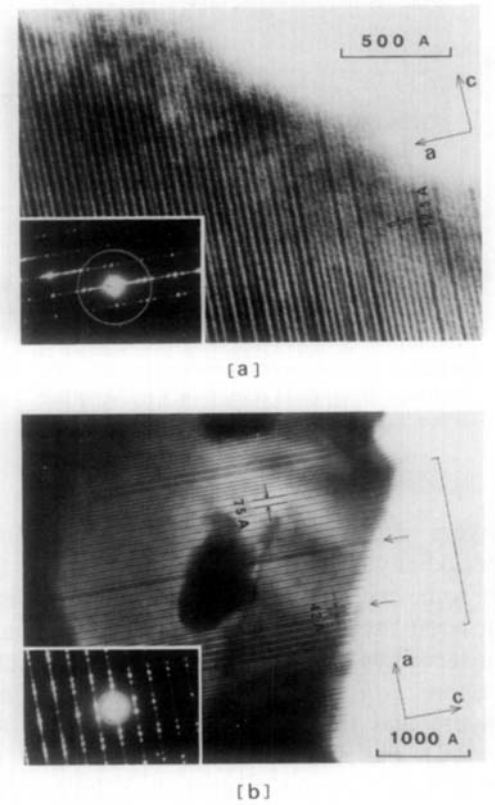

FIG. 3. Two examples of lattice fringe patterns with disordered interfringe spacings. The inset shows the corresponding $(h01)^*$ diffraction patterns. (a) Two-dimensional lattice fringe image. Interfringe spacing along c axis is constant (12.5 Å = c) while that along a axis is disordered. (b) An example of ordered intergrowths of $4a_0$ and $5a_0$ layers. The region of ordered intergrowth structure is shown in the figure. Arrows indicate the stacking faults in the $9a_0$ structure.

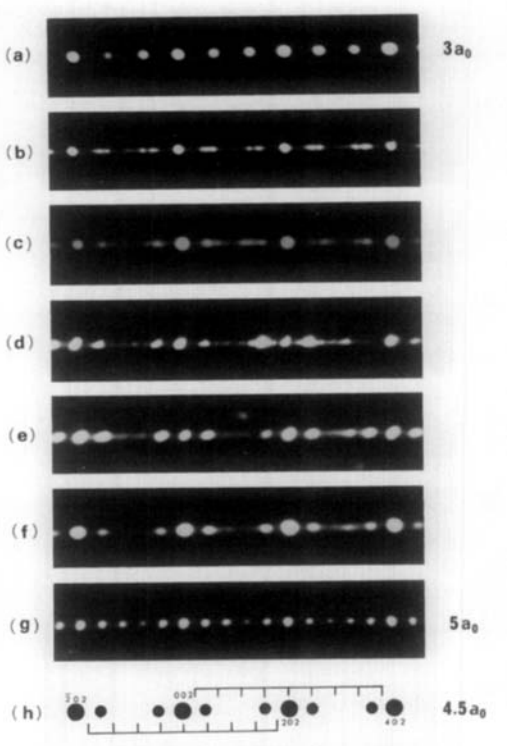

FIG. 4. Enlargements of diffraction patterns with diffuse streaks. Note the change in the position of intensity maxima. The schematic representation of the 4.5 a_0 diffraction pattern is shown in (h).

The positions of intensity maxima of diffuse streaks are seen to vary slightly from one diffraction pattern to another when carefully measured, as shown in Fig. 4 where they are compared with superlattice spots of β-$Ba_9Fe_4S_{15}$ ($3a_0$) and $Ba_{15}Fe_7S_{25}$ ($5a_0$). The corresponding lattice fringes (bright-field image) are shown in Fig. 5. In the structure images of the crystal giving the diffraction patterns (b) and (c) of Fig. 4, interfringe spacings are an irregular mixture of three periodicities, $3a_0$, $4a_0$, $5a_0$. In some regions bundles of fringes with a $3a_0$ periodicity appear but such regions are narrow. As a whole, the sequence of interfringe spacings is random.

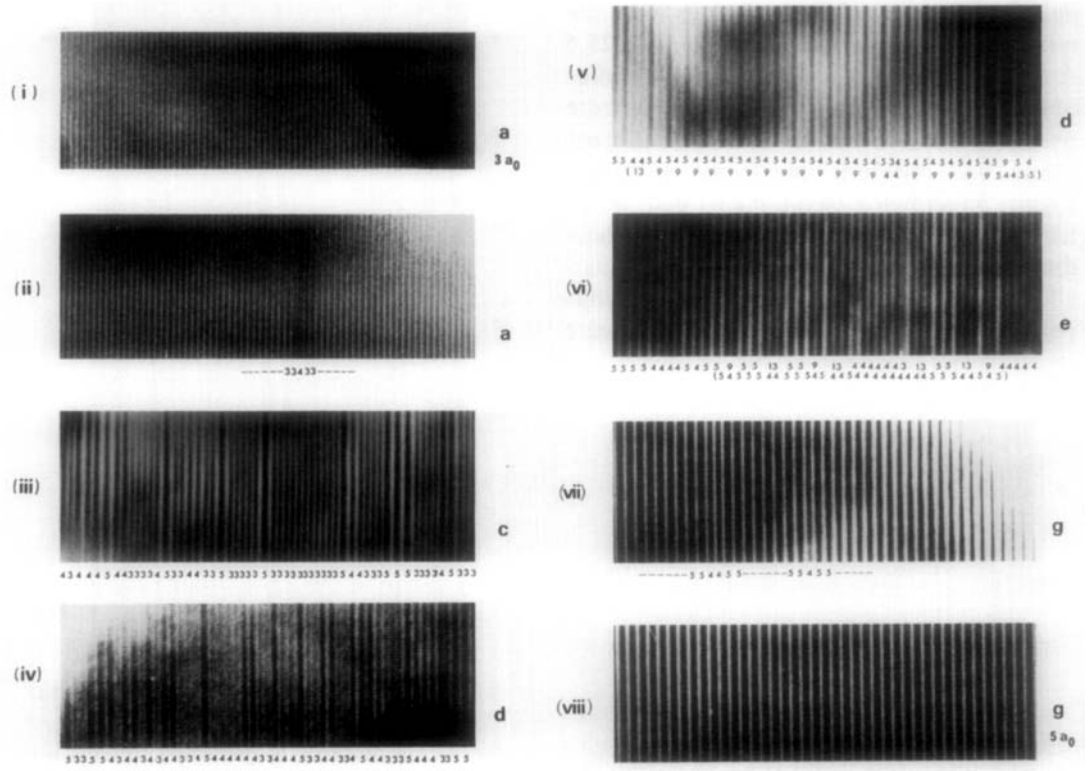

FIG. 5. Enlargements of lattice fringe images corresponding to the diffraction patterns (a), (c), (d), (e), and (g) in Fig. 4. Interfringe spacings are shown as the multiple numbers of a_0 ($\simeq$8.5 Å). Another possible stacking is also shown in parentheses. The two lattice images corresponding to one diffraction pattern are those of different areas of a fragment.

The intensity maxima of diffuse streaks in the diffraction patterns (d), (e), and (f) of Fig. 4 are relatively intense ones, comparable with main spots. Their positions are irrational, that is to say, a spacing anomaly or an incommensurate spacing was observed. The corresponding periodicity is $4.5a_0$ as shown in the figure. In general, incommensurate spacings are considered to be due to the presence of the regular mixture of two different periodicities (*9, 10*). In this case, a 1 : 1 mixture of $4a_0$ and $5a_0$ periodicities is expected. In fact, observed lattice fringes show the intergrowth structure of $4a_0$ and $5a_0$ periodicities. Often, the arrangement of interfringe spacings is disordered and the ratio of the number of layers with $4a_0$ periodicity to that with $5a_0$ periodicity is nearly 1 : 1 as shown in Fig. 5. In some crystals, however, a region with an ordered arrangement of $4a_0$ and $5a_0$ was observed as shown in Figs. 3b and 5. Such regions consist of alternating $4a_0$ and $5a_0$ layers and the total periodicity is 75 Å ($\simeq 9a_0$). The regions did not extend over a wide range and are at most 20–30 layers. In this region, also, some defects were observed as shown in Fig. 3b.

Discussion

1. *A Model for the Intergrowth Structure*

Electron microscopic observations show

a complex intergrowth structure in $Ba_3Fe_{1+x}S_5$ with a composition x intermediate between those of 0.33 (β-$Ba_9Fe_4S_{15}$) and 0.40 ($B_{15}Fe_7S_{25}$). The intergrowth structure consists of three structure variants, $3a_0$, $4a_0$, and $5a_0$. The $3a_0$ and $5a_0$ layers correspond to the structure of β-$Ba_9Fe_4S_{15}$ and $Ba_{15}Fe_7S_{25}$, respectively. The $4a_0$ layers appear as defects or stacking faults in the $3a_0$ and $5a_0$ structures as shown in Fig. 5(ii, vii). The region of $4a_0$ layers in the intergrowth structure is very narrow up to 4 or 5 layers. The observed intergrowth structure can be, basically, interpreted as the random intermingling of $3a_0$ and $5a_0$ structures. However, the existence of $4a_0$ layers precludes the interpretation of the intergrowth structure by the simple intermingling model. The problem to be solved is the appearance of the structure with $4a_0$ periodicity in the disordered intergrowth structure. The superstructure of the $Ba_{3p}Fe_qS_{5p}$ series occurs due to the variation of Fe occupation number α in successive rings of the Ba_3S_5 framework along the a axis. The sequence of α in the $4a_0$ layer must be closely related to that in β-$Ba_9Fe_4S_{15}$ ($3a_0$) and $Ba_{15}Fe_7S_{25}$ ($5a_0$); that is, the random intermingling of $3a_0$ and $5a_0$ structures seems to cause the exclusion or insertion in the sequence of α and, as a result, the $4a_0$ structure appears.

As a model for the microscopic disordered intergrowth structure, we postulate that the intergrowth structure may originate from the "random" sequence of α within the limit of a rule based on the intermingling of $3a_0$ and $5a_0$ structures. It is reasonable to assume that the rule can be derived from the crystal structures of β-$Ba_9Fe_4S_{15}$ ($3a_0$) and $Ba_{15}Fe_7S_{25}$ ($5a_0$) and that the resultant sequence must correspond to the composition intermediate between those of the two structures. These conditions will minimize the free energy of the system.

From the sequence of α in β-$Ba_9Fe_4S_{15}$ and $Ba_{15}Fe_7S_{25}$, i.e., –2–3–3–2–3–3–· · · and –2–3–4–3–2–2–3–4–3–2–· · · a rule for the sequence along the a axis can be deduced. When the α in two successive rings is determined, the α in the next ring along the a axis is determined as follows:

α in the two successive rings	α in the next ring
4–3	2
3–4	3
3–3	2
3–2	3 or 2
2–3	4 or 3
2–2	3

Moreover, we have to consider the configuration of Fe in a near-neighboring array (the B array in Fig. 1) of rings along the a axis. For example, a ring with four Fe in the A array has four rings with two Fe in each ring in near-neighbor B arrays. There are six types of fundamental blocks as shown in Fig. 6a, which appear in the $3a_0$ and $5a_0$ structures. Each of these is hereafter to be denoted as $^{2}4^{2}$, $^{3}3^{2}$, $^{2}3^{3}$, $^{3}2^{3}$, $^{3}2^{4}$, $^{4}2^{3}$.

From the consideration of the configuration of Fe in near-neighbor arrays of rings, the random arrangement of lattice fringes originates from the random stacking of six blocks within the limit of a rule that is represented in Fig. 6b by a map. The left cycle (thick line) corresponds to the $5a_0$ structure and the right one (thin line) to the $3a_0$ structure. The sequence of the blocks in a crystal is determined by the random walking along the direction of the arrows in the map. It is noted that this map satisfies the above-mentioned rule derived from the α sequence only in the A array.

Now, let us show the result of block sequence obtained by the "random walking" in the map, as follows:

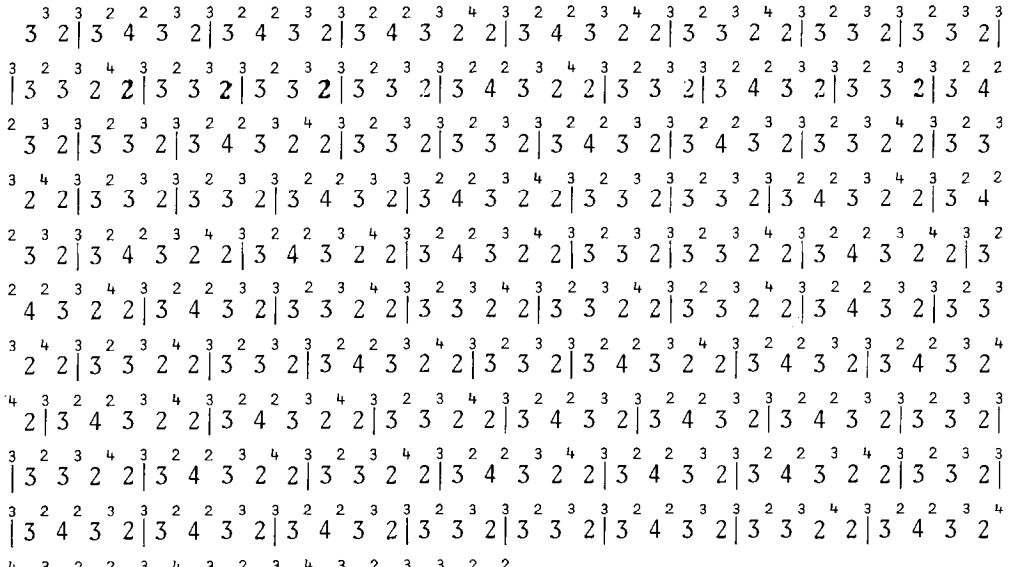

Here, for example, $---{}^{3}2^{4}{-}^{4}2^{3}{-}^{3}3^{2}---$ is abbreviated to $---{}^{3}2^{4}2^{3}3^{2}---$. The line division between figures shows the unit cell of $3a_0$, $5a_0$, and $4a_0$. The unit cell sequence obtained in this case is as follows:

4 4 5 5 4 3 3 4 3 3 3 5 3 4 3 4 3 5 3 3 4 4 4 4 3 3 4 5
3 3 5 4 5 5 5 3 4 5 5 4 4 4 4 4 4 4 4 3 5 3 5 4 5 5 5 4
4 4 4 3 4 5 4 5 4 5 3 3 4 4 3 3 4 4 5 5 4 3 . . . .

Thus, we could estimate the structure of the $4a_0$ layers appearing in the intergrowth structure and hence the origin of the random arrangement of lattice fringes shown in Figs. 3 and 5 was understood in principle. The block sequence in the $4a_0$ layer is $|{}^{3}3^{2}4^{2}3^{3}2^{4}|$ or $|{}^{3}3^{2}3^{3}2^{4}2^{3}|$, which are the same structure with a shift of origin as the only difference. Its chemical formula is $Ba_{24}Fe_{11}S_{40}$ and its composition, $x = 0.375$, is intermediate between 0.33 ($3a_0$) and 0.40 ($5a_0$). This $4a_0$ structure corresponds to the $5a_0$ structure missing a $^{2}4^{2}$ block or the $3a_0$ structure with a $^{2}4^{2}$ block inserted.

It is obvious that the average composition of the crystal obtained by infinite random walking is $Ba_3Fe_{11/8}S_5$, i.e., $3a_0 : 5a_0 = 1 : 1$. In order to specify the average composition, we have to determine the probability of each path at the diverging points $^{2}3^{3}$ and $^{3}3^{2}$. For example, in the case of 5 : 3 composition of β-$Ba_9Fe_4S_{15}$ ($3a_0$) and $Ba_{15}Fe_7S_{25}$ ($5a_0$), i.e., $Ba_3Fe_{41/30}S_5$ ($x = 0.367$), the path probabilities are as follows:

$$^{3}3^{2} \xrightarrow{\beta_1} {}^{2}3^{3} \qquad \beta_1 = \tfrac{5}{8}$$

$$^{3}3^{2} \xrightarrow{\beta_2} {}^{2}4^{2} \qquad \beta_2 = \tfrac{3}{8}$$

$$^{2}3^{3} \xrightarrow{\beta_3} {}^{3}2^{4} \qquad \beta_3 = \tfrac{3}{8}$$

$$^{2}3^{3} \xrightarrow{\beta_4} {}^{3}2^{3} \qquad \beta_4 = \tfrac{5}{8}.$$

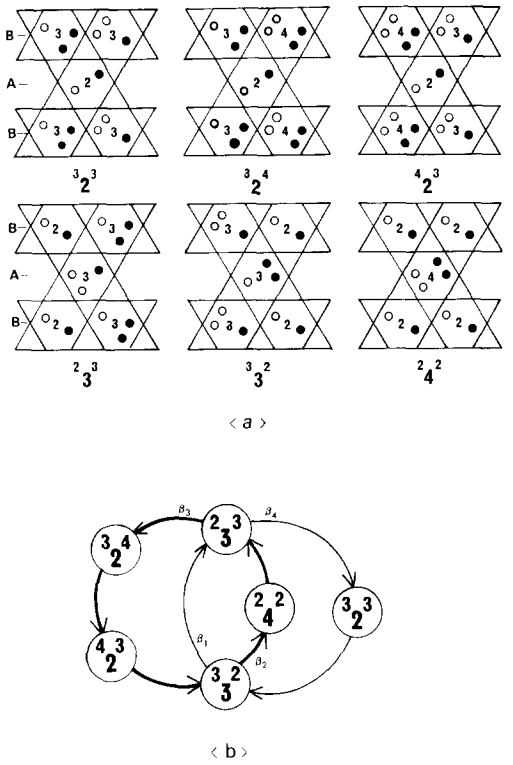

FIG. 6 (a) Fundamental blocks in the structure of the $Ba_3Fe_{1+x}S_5$ system. Each block is hereafter denoted as $^{3}2^{3}$, $^{3}2^{4}$, $^{4}2^{3}$, $^{3}3^{2}$, $^{2}3^{3}$, $^{2}4^{2}$, respectively. (b) The map of possible stacking sequence of these six blocks derived from the sequence in β-$Ba_9Fe_4S_{15}$ and $Ba_{15}Fe_7S_{25}$. The thick solid line route corresponds to the sequence in $Ba_{25}Fe_7S_{25}$ and the thin solid line to that in β-$Ba_9Fe_4S_{15}$. β in the figure shows the path probability to specify the average composition of a crystal, which shows random lattice fringes.

The result of random walking under these conditions is shown in Fig. 7, together with the other two cases of $\beta_1 = \beta_2 = \beta_3 = \beta_4 = \frac{1}{2}$ ($Ba_3Fe_{11/8}S_5$, $x = 0.375$) and $\beta_1 = \beta_4 = \frac{1}{3}$, $\beta_2 = \beta_3 = \frac{2}{3}$ ($Ba_3Fe_{18/13}S_5$, $x = 0.384$). These random sequences show great similarity with the observed arrangement of interfringe spacings. The alternate sequence of $4a_0$ and $5a_0$ periodicities partially appears in Fig. 7c. This may correspond to the observed ordered intergrowth structure shown in Fig. 3b. Then, the block sequence and the chemical formula of the $9a_0$ structure were deduced as $^{2}_{1}3^{3}2^{4}2^{3}3^{2}4^{2}3^{3}2^{4}2^{3}3^{2}_{1}$ and $Ba_3Fe_{25/18}S_5$ ($x = 0.389$), respectively. It is notable that the removal of $^{2}4^{2}$ blocks from every other layer of the $5a_0$ structure gives us this block sequence for the $9a_0$ structure.

2. *Infinitely Adaptive Nature*

The disordered intergrowth structure similar to that in $Ba_3Fe_{1+x}S_5$ has often been observed in the narrow composition range between two members of a homologous series with different supercell periodicity, constructed by a structure principle. For example, in the V_nO_{2n-1} series, a syntactic intergrowth structure of two neighboring members, V_8O_{15} and V_9O_{17}, on a unit cell scale was recently reported (*12*). Such intergrowth structures are called "microsyntactic" intergrowth structures (*12, 13*). In $Ba_3Fe_{1+x}S_5$, intergrowth between β-$Ba_9Fe_4S_{15}$ and $Ba_{15}Fe_7S_{25}$ is assumed to be basically "microsyntactic." The uniqueness of this system is the appearance of $4a_0$ layers, which is due to the irregular sequence of Fe occupation in hexagonal rings along the a axis as mentioned above.

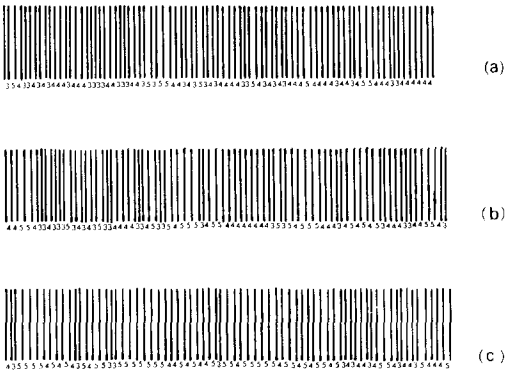

FIG. 7. Calculated stacking sequence under the conditions $\beta_1 = \beta_4 = \frac{5}{8}$, $\beta_2 = \beta_3 = \frac{3}{8}$ (a), $\beta_1 = \beta_2 = \beta_3 = \beta_4 = \frac{1}{2}$ (b), and $\beta_1 = \beta_4 = \frac{1}{3}$, $\beta_2 = \beta_3 = \frac{2}{3}$ (c). The chemical formulas are $Ba_{90}Fe_{41}S_{150}$ ($x = 0.367$), $Ba_{24}Fe_{11}S_{40}$ ($x = 0.375$), and $Ba_{39}Fe_{18}S_{65}$ ($x = 0.385$), respectively. Compare with lattice fringe images shown in Fig. 5.

The "microsyntactic" intergrowth often leads to the "adaptive" intergrowth (*5*, *6*), which is an ordered intergrowth of the two members. The observed ordered intergrowth region of $5a_0$ and $4a_0$ layers suggests the possibility of "adaptive" intergrowth in the $Ba_3Fe_{1+x}S_5$. In this system, the "infinitely adaptive" nature predicted by Cohen *et al.* (*2*) was not observed, but it is expected that "adaptive" intergrowth consisting of three structure variants, $3a_0$, $4a_0$, and $5a_0$, can be acquired after long-time annealing at low temperatures in the narrow composition range between $x = 0.333$ and 0.40.

References

1. J. T. LEMLEY, J. M. JENKS, J. T. HOGGINS, Z. ELIEZER, AND H. STEINFINK, *J. Solid State Chem.* **16,** 117 (1976).
2. S. COHEN, L. E. RENDON-DIAZMIRON, AND H. STEINFINK, *J. Solid State Chem.* **25,** 179 (1978).
3. I. E. GREY, *J. Solid State Chem.* **11,** 128 (1974).
4. J. T. HOGGINS AND H. STEINFINK, *Acta Crystallogr. Ser. B* **33,** 673 (1977).
5. J. S. ANDERSON, *J. Chem. Soc. Dalton Trans.* 1107 (1973).
6. J. S. ANDERSON, *J. Phys. (Paris)* **38,** C7-17 (1977).
7. I. E. IGLESIAS AND H. STEINFINK, *Z. Kristallogr. Kristallgeometrie Kristallphys. Kristallchem.* **142,** 398 (1975).
8. C. B. SHOEMAKER, *Z. Kristallogr. Kristallgeometrie Kristallphys. Kristallchem.* **137,** 225 (1973).
9. K. FUJIWARA, *J. Phys. Soc. Japan* **12,** 7 (1957).
10. C. CONDE, C. MANOLIKAS, D. VAN DYCK, P. DELAVIGRETTE, J. VAN LANDUYT, AND S. AMELINCKX, *Mater. Res. Bull.* **13,** 1055 (1978).
11. J. T. HOGGINS, I. E. RENDON-DIAZMIRON, AND H. STEINFINK, *J. Solid State Chem.* **21,** 79 (1977).
12. Y. HIROTSU, S. P. FAILE, AND H. SATO, *Mater. Res. Bull.* **13,** 895 (1978).
13. H. SATO AND Y. HIROTSU, *Mater. Res. Bull.* **11,** 1307 (1976).